# Moment analysis of rf parallel-plate-discharge simulations using the particle-in-cell with Monte Carlo collisions technique

M. Surendra and M. Dalvie
*IBM Thomas J. Watson Research Center, P.O. Box 218, Yorktown Heights, New York 10598*
(Received 19 April 1993)

Self-consistent simulations of rf parallel-plate discharges using the particle-in-cell with Monte Carlo collisions technique are employed to calculate explicitly the terms in moment or fluid equations that are derived from the Boltzmann equation. Isotropic electron–neutral-species elastic and ionizing collisions and ion–neutral-species charge-exchange collisions are included in the simulation. Results indicate that the convective term in the electron momentum balance can be neglected over a wide range of conditions. This approximation is also reasonable for ions when the sheaths are collisional. An analysis of terms in the electron energy balance indicate that heat conduction is important. However, the common expressions for heat conduction, such as the Fourier heat conduction, are not particularly accurate. The primary components of electron heating come from friction (collisional or Ohmic) and pressure work terms. For the particular model gas considered in this study, the collisional term is dominant for conditions when the product of pressure and gap is greater than 0.4 Torr cm.

PACS number(s): 52.80.Pi, 52.25.Fi, 52.65.+z

## I. INTRODUCTION

Glow discharges created by the application of rf voltages are routinely used in the materials processing industry. These discharges are, in general, complex systems that are difficult to analyze. Thus, there has been a substantial effort in recent years to model these systems self-consistently. A wide variety of models have been used, ranging from analytic models [1–5], fluid (or moment) models [6–17], hybrid techniques [18–21], to full numerical solutions of the Boltzmann equation [22] and particle methods [23–30]. Kinetic level simulations such as direct solutions to the Boltzmann equation, or particle-in-cell with Monte Carlo collisions (PIC-MCC) are attractive since they provide detailed kinetic information about the electrons and ions (velocity distributions) in the discharge. However, these types of simulations are computationally very expensive, and hence may be impractical for modeling large two or three-dimensional glow discharge reactors. Fluid models are, on the other hand, typically much faster than kinetic level simulations. One important drawback of fluid methods is that assumptions and approximations (regarding the distribution functions) of sometimes questionable validity are required.

In this paper we present a study of common assumptions and approximations in fluid (or moment) models. Terms in the electron and ion moment equations are evaluated directly from a PIC-MCC simulation. This procedure allowed us to identify important terms in the equations and also check the validity of assumptions. The moment approach also allows us to examine the importance of collisional versus collisionless contributions to electron heating. Furthermore, we present an analytic treatment to predict the possible presence and magnitude of field reversals in sheaths, which have recently been shown to be important in some rf discharges [29].

## II. PARTICLE-IN-CELL WITH MONTE CARLO COLLISIONS TECHNIQUE

A description of the PIC-MCC technique used here has been reported elsewhere [25,26]. The simulations were performed for a one-dimensional (spatial) rf discharge between parallel plates separated by a 4-cm gap. Since the system is axisymmetric, only two velocity dimensions are required, $v_x$ (velocity parallel to the discharge axis) and $v_\perp$ (speed perpendicular to the $x$ axis). A very simple model gas (loosely based on hydrogen) with an ionic mass of 2 amu is used in this study. The electron–neutral-species processes included are elastic scattering and ionization. The total electron–neutral-species scattering cross section ($\sigma_{\rm tot}$) is given by $\sigma_{\rm tot}=K_{\rm tot}/v_e$, where $v_e$ is the electron speed ($v^2=v_x^2+v_\perp^2$), and the rate constant $K_{\rm tot}$ is $5\times10^{-14}$ m$^3$/s. All collisions with incident electron energy ($\varepsilon_e$) greater than the ionization threshold ($\varepsilon_{\rm ion}=16$ eV) are taken to be ionizing collisions. The energy of the ejected electron in an ionizing collision is determined according to a distribution presented previously [24]. Electrons are scattered isotropically (in the laboratory frame of reference) after all collisions. Ions charge exchange with the neutral species with a constant cross section ($\sigma_{\rm chx}$) of $1\times10^{-19}$ m$^2$. The background neutral-species velocity is chosen randomly from a Maxwellian distribution with a temperature of 0.026 eV. Note that the ion–neutral-species relative velocity is used to calculate the collision probability. Ions created in ionizing events are assigned velocities chosen from the neutral-species velocity distribution. Boundaries are assumed to be perfectly absorbing for both electrons and ions. Secondary-electron emission due to ion bombardment is neglected.

We use 40 000–80 000 particles and 400 spatial cells in

 

the simulations. The time step (0.01–0.1 ns) is small enough to resolve the electron plasma frequency.

## III. MOMENTS OF THE BOLTZMANN EQUATION

In this study we focus on the first three moments of the Boltzmann equation for electron transport and the first two moments for ion transport. Details of the derivation of the moment equations are presented elsewhere [31,32] and are not repeated here. Briefly, the moment equations are obtained by multiplying the Boltzmann equation (written here for one spatial dimension $x$, and two velocity dimensions $v_x$ and $v_\perp$),

$$\frac{\partial f}{\partial t}+v_x\frac{\partial f}{\partial x}+\frac{qE}{m}\frac{\partial f}{\partial v_x}-\left[\frac{\partial f}{\partial t}\right]_{\text{coll}}=0 \tag{1}$$

with increasing powers of velocity and integrating over velocity space. In the above equation the distribution function $f$, is a function of $(x,v_x,v_\perp,t)$, where $t$ denotes time, while $E$, $q$, and $m$ are the electric field (parallel to $x$ axis), species charge and mass, respectively. The last term on the left-hand side is the collision integral. The zeroth moment equation is species conservation, while the first moment ($mv_x$) equation is momentum conservation. There are two second moment equations we can consider, energy ($\frac{1}{2}mv_x^2+\frac{1}{2}mv_\perp^2$), and parallel energy ($\frac{1}{2}mv_x^2$) conservation.

In the derivation of the moment equations, we assume that the neutral background is cold and that the rate constant for electron–neutral-species elastic scattering is approximately equal to $K_{\text{tot}}$. Furthermore the energy loss due to elastic recoil has been ignored in the electron momentum and parallel energy balances. These assumptions introduce negligible errors. Note that the moment of any quantity $\theta$ (such as velocity) is defined by $n\langle\theta\rangle\equiv\int\theta f(x,v_x,v_\perp,t)d\mathbf{v}$,

$$\frac{\partial n_e}{\partial t}+\frac{\partial(n_e u_e)}{\partial x}-S_{\text{ion}}=0\ , \tag{2}$$

$$\frac{\partial(n_e m_e u_e)}{\partial t}+\frac{\partial(n_e m_e u_e^2)}{\partial x}+\frac{\partial(n_e kT_{ex})}{\partial x}+en_eE+n_e m_e n_n\langle v_{ex}v_e\sigma_{\text{tot}}^m\rangle=0\ , \tag{3}$$

$$\frac{\partial(\frac{1}{2}n_e m_e u_e^2+\frac{3}{2}n_e kT_e)}{\partial t}+\frac{\partial(\frac{1}{2}n_e m_e u_e^3+\frac{3}{2}n_e kT_e u_e)}{\partial x}+\frac{\partial(n_e kT_{ex}u_e)}{\partial x}+\frac{\partial Q_e}{\partial x}+en_e u_e E+\frac{m_e}{m_n}n_e m_e n_n\langle v_e^3\sigma_{\text{tot}}^m\rangle+\varepsilon_{\text{ion}}S_{\text{ion}}=0\ , \tag{4}$$

$$\frac{\partial(\frac{1}{2}n_e m_e u_e^2+\frac{1}{2}n_e kT_{ex})}{\partial t}+\frac{\partial(\frac{1}{2}n_e m_e u_e^3+\frac{1}{2}n_e kT_{ex}u_e)}{\partial x}+\frac{\partial(n_e kT_{ex}u_e)}{\partial x}+\frac{\partial Q_{ex}}{\partial x}+en_e u_e E+\frac{1}{2}n_e m_e n_n\left\langle\left[\frac{3}{2}v_{ex}^2-\frac{1}{2}v_e^2\right]v_e\sigma_{\text{tot}}^v\right\rangle+\frac{1}{3}\varepsilon_{\text{ion}}S_{\text{ion}}=0\ , \tag{5}$$

$$\frac{\partial n_+}{\partial t}+\frac{\partial(n_+u_+)}{\partial x}-S_{\text{ion}}=0\ , \tag{6}$$

$$\frac{\partial(n_+m_+u_+)}{\partial t}+\frac{\partial(n_+m_+u_+^2)}{\partial x}+\frac{\partial(n_+kT_{+x})}{\partial x}-en_+E+n_+m_+n_n\langle v_{+x}v_+\sigma_{\text{chx}}\rangle=0\ . \tag{7}$$

Equations (2), (3), (4), and (5) are electron species, momentum, energy, and parallel energy conservation, respectively, while Eqs. (6) and (7) are ion species and momentum conservation, respectively. Subscripts $e$, $+$, and $n$ refer to electrons, ions, and neutral species, respectively. $n$ is species density and $u$ is species average velocity, while $e$ is the electronic charge and $k$ is Boltzmann's constant. The "temperature" is defined as $kT\equiv\frac{1}{3}m\langle w^2\rangle$, while the "$x$ temperature" is given by $kT_x\equiv m\langle w_x^2\rangle$, where $\mathbf{w}$ is the random part of species velocity ($\mathbf{w}\equiv\mathbf{v}-\mathbf{u}$). Electron heat conduction fluxes are defined as $Q_e\equiv\frac{1}{2}m_e n_e\langle w_e^2 w_{ex}\rangle$, and $Q_{ex}\equiv\frac{1}{2}m_e n_e\langle w_{ex}^3\rangle$. The ionization rate, $S_{\text{ion}}$ is given by $S_{\text{ion}}=n_e n_n\langle v\sigma_{\text{ion}}\rangle$. $\sigma_{\text{tot}}^m$ and $\sigma_{\text{tot}}^v$ are the momentum transfer and viscosity cross sections, respectively [33]. Under the assumption of isotropic electron–neutral-species scattering, $\sigma_{\text{tot}}^m=\sigma_{\text{tot}}$, and $\sigma_{\text{tot}}^v=\frac{2}{3}\sigma_{\text{tot}}$. Furthermore, given that $\sigma_{\text{tot}}=K_{\text{tot}}/v_e$, the friction terms in Eqs. (3)–(5) simplify to

$$n_e m_e n_n\langle v_{ex}v_e\sigma_{\text{tot}}^m\rangle=n_e m_e n_n K_{\text{tot}}\langle v_{\text{ex}}\rangle=n_e m_e\nu_e u_e\ , \tag{8}$$

$$\frac{m_e}{m_n}n_e m_e n_n\langle v_e^3\sigma_{\text{tot}}^m\rangle=\frac{m_e}{m_n}n_e m_e n_n K_{\text{tot}}\langle v_e^2\rangle=\frac{2m_e}{m_n}\nu_e(\tfrac{1}{2}n_e m_e u_e^2+\tfrac{3}{2}n_e kT_e)\ , \tag{9}$$

$$\frac{1}{2}n_e m_e n_n\langle(\tfrac{3}{2}v_{ex}^2-\tfrac{1}{2}v_e^2)v_e\sigma_{\text{tot}}^v\rangle=\frac{1}{2}n_e m_e n_n K_{\text{tot}}\langle(v_{ex}^2-\tfrac{1}{3}v_e^2)\rangle=\nu_e(\tfrac{1}{3}n_e m_e u_e^2+\tfrac{1}{2}n_e kT_{ex}-\tfrac{1}{2}n_e kT_e)\ . \tag{10}$$

The electron collision frequency $\nu_e$, is defined as $\nu_e \equiv n_n \langle v_e \sigma_{\rm tot} \rangle = n_n K_{\rm tot}$. Given that the ions undergo only charge-exchange collisions with constant $\sigma_{\rm chx}$, the collision term in Eq. (7) can be written as

$$n_+ m_+ n_n \langle v_{+x} v_+ \sigma_{\rm chx} \rangle = n_+ m_+ n_n \sigma_{\rm chx} \langle v_{+x} | v_{+x} | \rangle \ . \tag{11}$$

Velocity moments are obtained from the PIC-MCC simulation by weighting particle positions and powers of velocities to the spatial grid. The quantities obtained directly from the simulation are $E$, $n$, $n\langle v_x \rangle$, $n\langle v^2 \rangle$, $n\langle v_x^2 \rangle$, $n\langle v^2 v_x \rangle$, $n\langle v_x^3 \rangle$, and $S_{\rm ion}$ (this quantity was obtained by weighting ionization events to the spatial grid). Note that the third moment is not needed for ions since we are not looking at ion heat conduction. The various quantities of interest can then be obtained since $\langle v_x \rangle = u$, $\langle v^2 \rangle = u^2 + \langle w^2 \rangle$, $\langle v_x^2 \rangle = u^2 + \langle w_x^2 \rangle$, $\langle v^2 v_x \rangle = \langle v^2 \rangle u + 2\langle w_x^2 \rangle u + \langle w^2 w_x \rangle$, and $\langle v_x^3 \rangle = \langle v_x^2 \rangle u + 2\langle w_x^2 \rangle u + \langle w_x^3 \rangle$.

## IV. CLOSURE RELATIONSHIPS AND COMMON ASSUMPTIONS

Closure relationships are required to terminate the series of moment equations, since each moment equation involves higher-velocity moments or special moments such as the ionization rate. In fluid simulations, $S_{\rm ion}$ is typically expressed as a function of the local electric field [7] or a characteristic electron energy [6,16,34]. Rate constants are obtained either from swarm or drift tube data [7,16], or by assuming a distribution function (e.g., Maxwellian distribution) and integrating known cross sections over velocity space [34]. Rate constants for other electron–neutral-species inelastic processes are obtained in a similar fashion. We note that in hybrid kinetic-fluid simulations, rate data are calculated with Monte Carlo methods that are coupled to fluid models for charged particle transport [18–20]. It should be pointed out that if $\sigma_{\rm tot} \neq K_{\rm tot}/v_e$, further assumptions involving the friction terms in Eqs. (3)–(5) are required. For example, the friction term in Eq. (3) is often approximated by $n_e m_e n_n \langle v_{ex} v_e \sigma_{\rm tot}^m \rangle \approx n_e m_e \nu_e u_e$ [31]. Another closure relationship that is required for the electron moment equations is related to heat conduction. The two most common approaches here are to assume Fourier heat conduction, $Q_e^{\rm Fo} = -\kappa_e \partial T_e/\partial x$, where $\kappa_e \sim n_e k (kT_e/m_e \nu_e)$ (a similar expression can be written for $Q_{ex}$) [6,12–14,16,34], or ignore heat conduction in the energy equations [Eqs. (4) and (5)] [9,17,35]. In addition to the required closure relationships, assumptions are often made to simplify and/or reduce the number of differential equations. One approximation that is almost universally used is $kT_{ex} \approx kT_e$. This assumption is very convenient since there is then no need to solve for $kT_{ex}$ and Eq. (5) becomes unnecessary. This assumption is generally quite good in situations where conditions that normally give rise to significant anisotropy in the electron velocity distribution, such as magnetic fields or secondary electron emission from electrodes, are not important. It is also common practice to drop drift energy terms in Eq. (4) since typically $\frac{3}{2}kT_e \gg \frac{1}{2}m_e u_e^2$. The electron momentum balance [Eq. (3)] is usually reduced to an algebraic expression for $u_e$ by dropping the acceleration $[\partial(n_e m_e u_e)/\partial t]$ and convection $[\partial(n_e m_e u_e^2)/\partial x]$ terms. Furthermore, the pressure term $[\partial(n_e kT_e)/\partial x]$ is often simplified to $[kT_{e,\rm avg} \partial n_e/\partial x]$, where $kT_{e,\rm avg}$ is an approximate electron temperature [7,12–14,16],

$$u_e = -\frac{e}{m_e \nu_e} E - \frac{1}{n_e m_e \nu_e} \frac{\partial (n_e kT_{ex})}{\partial x} \ , \tag{12}$$

$$u_e = -\frac{e}{m_e \nu_e} E - \frac{kT_{e,\rm avg}}{n_e m_e \nu_e} \frac{\partial n_e}{\partial x} \ . \tag{13}$$

Equation (13) is commonly known as the drift-diffusion approximation, where the mobility $\mu_e$ is given by $\mu_e = e/m_e \nu_e$ and the diffusivity $D_e$ is given by $D_e = kT_{e,\rm avg}/m_e \nu_e$.

Closure for the ion moment equations is achieved by making assumptions about the behavior of $\langle v_{+x}^2 \rangle$ [Eqs. (7) and (11)]. One possibility is to assume that the behavior of the ion velocity distribution function is in approximate equilibrium with the local instantaneous electric field. The ion velocity distribution for this situation $[f(v_{+x}) \propto \exp(-v_{+x}^2 \sigma_{\rm chx} n_n m_+ / 2eE)]$ results in [36]

$$\langle v_{+x}^2 \rangle = u_+^2 + \langle w_{+x}^2 \rangle = \frac{\pi}{2} u_+^2 \ . \tag{14}$$

The full momentum balance is sometimes solved in fluid simulations of rf discharges [15,34]. In many circumstances the drift-diffusion approximation is also used for ions [6,7,9–13],

$$u_+ = \frac{e}{m_+ \nu_+} E - \frac{kT_{+,\rm avg}}{n_+ m_+ \nu_+} \frac{\partial n_+}{\partial x} \ . \tag{15}$$

The ion collision frequency $\nu_+$ is often expressed as a function of the local instantaneous field. For the case considered here $\nu_+ = (\pi \sigma_{\rm chx} n_n e |E|/2m_+)^{1/2}$ [substitute Eqs. (14) and (11) into Eq. (7) with time- and space-derivative terms set to zero]. $kT_{+,\rm avg}$ in Eq. (15) is frequently approximated by the neutral temperature $kT_n$. In an effort to capture the time-varying nature of the problem, some approaches solve a simplified ion momentum equation [Eq. (7) with space-derivative terms set to zero] for a drift velocity which is used in place of $eE/m_+ \nu_+$ in Eq. (15) [14,16,17].

## V. RESULTS AND DISCUSSION

The discharge gap is 4 cm and the applied rf voltage is 200 V for all simulations. The left electrode is powered with voltage $V = \tilde{V}_{\rm rf} \sin(\omega_{\rm rf} t)$, and the right electrode is grounded. We present results from six cases here: 12 MHz, 400 mtorr; 12 MHz, 200 mtorr; 12 MHz, 100 mtorr; 30 MHz, 100 mtorr; 30 MHz, 50 mtorr; 30 MHz, 25 mtorr.

### A. Electron moments

As discussed in the previous section, a common assumption in many fluid simulations is

$kT_{ex} \approx kT_e \gg \frac{1}{2} m_e u_e^2$. Results from the simulation at 12 Mhz, 100 mtorr [Figs. 1(a)–1(c)] indicate that this is a reasonably good approximation. The approximation improves with pressure [Figs. 1(d)–1(f)]. The greatest differences between $kT_e$ and $kT_{ex}$ are apparent in the sheath regions. This is not surprising, since the effect of the varying electric field, which drives the anisotropy in the velocity distribution, is greatest there. Since the anisotropy should relax with a time constant $\sim 1/\nu_e$ [Eqs. (5) and (10)], it appears that the assumption should be reasonable for $\nu_e \geq \omega_{\rm rf}$ the applied rf frequency. This condition is consistent with the results of simulations considered here. In the lowest-pressure case (30 MHz, 25 mtorr) where $\nu_e = 4 \times 10^7 \text{s}^{-1}$, $kT_{ex}$ is sometimes almost twice as great as $kT_e$ in the sheath regions. Note that this condition applies for situations where secondary-electron emission is unimportant.

The ionization rate obtained with the simulation is shown for two cases (12 MHz, 100 mtorr and 12 MHz, 400 mtorr) in Figs. 2(a) and 2(c). For comparison we also show in Figs. 2(b) and 2(d) the corresponding ionization rates $S_{\rm ion}^{\rm Max}$, assuming the electrons follow a Maxwellian distribution with a temperature $T_e^{\rm Max}(x,t)$, that is equal to $T_e(x,t)$ from the simulations. The electron density from the simulations is also used in this calculation,

$$S_{\rm ion}^{\rm Max} = n_e n_n K_{\rm tot} [(2\varepsilon_{\rm ion}/\pi k T_e^{\rm Max})^{1/2} \exp(-\varepsilon_{\rm ion}/kT_e^{\rm Max}) + \text{erfc}(\sqrt{\varepsilon_{\rm ion}/kT_e^{\rm Max}})] \ . \quad (16)$$

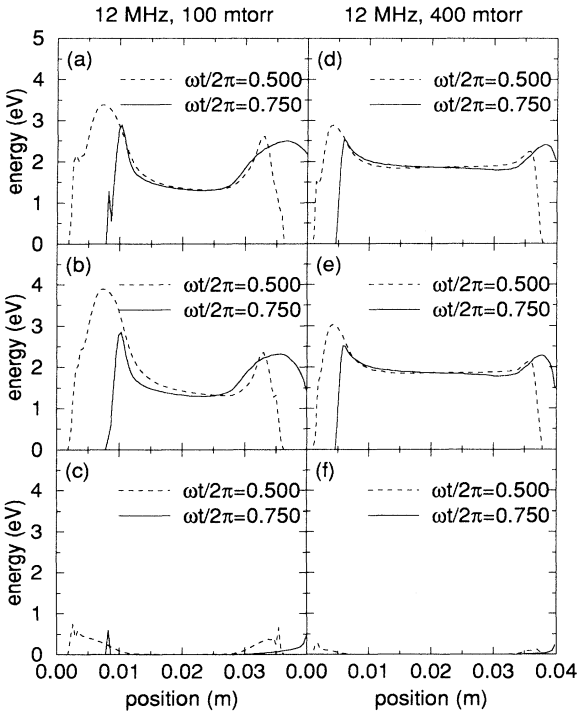


FIG. 1. Electron "temperature," "$x$ temperature," and drift energy: (a) $kT_e$ (12 MHz, 100 mtorr); (b) $kT_{ex}$ (12 MHz, 100 mtorr); (c) $\frac{1}{2} m_e u_e^2$ (12 MHz, 100 mtorr); (d) $kT_e$ (12 MHz, 400 mtorr); (e) $kT_{ex}$ (12 MHz, 400 mtorr); and (f) $\frac{1}{2} m_e u_e^2$ (12 MHz, 400 mtorr). The data are shown at two times in the rf cycle.

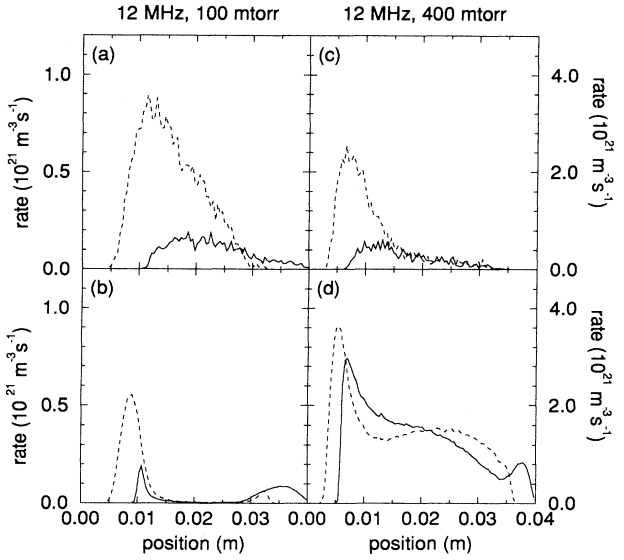


FIG. 2. Ionization rate obtained from simulation or calculated assuming Maxwellian distribution: (a) $S_{\rm ion}$ from simulation (12 MHz, 100 mtorr); (b) $S_{\rm ion}^{\rm Max}$ assuming Maxwellian EEDF (12 MHz, 100 mtorr); (c) $S_{\rm ion}$ from simulation (12 MHz, 400 mtorr); and (d) $S_{\rm ion}^{\rm Max}$ assuming Maxwellian EEDF (12 MHz, 400 mtorr). The data are shown at two times in the rf cycle.

The agreement between $S_{\rm ion}$ and $S_{\rm ion}^{\rm Max}$ is quite poor for both cases in Fig. 2, and is not any better for any of the other cases considered here. We note that a comparison of $S_{\rm ion}$ with rates calculated using swarm parameters for the model gas [37] (ionization rate coefficient correlated with either the local electric field or average electron energy in the simulations) is also unsatisfactory. This is not surprising since the electron-energy distribution function (EEDF) (see Fig. 3) does not resemble a Maxwellian distribution or a distribution obtained from a swarm simulation. Recent results indicate that EEDF's in rf discharges are quite complicated and are not easily modeled with well-characterized distribution functions (e.g., Maxwellian or from swarm calculations) [28,29,38,39]. The large modulation in the part of the EEDF's above $\varepsilon_{\rm ion}$ is not reflected in variation of $kT_e$ is the central region of the discharge. However, it is the behavior of this part of the EEDF that determines the spatial and temporal variation of the ionization rate. Thus, although $kT_e$ in the center of the discharge is lower at 100 mtorr ($\sim 1.3$ eV) than it is at 400 mtorr ($\sim 1.9$ eV), $S_{\rm ion}/n_e$ in the same region is larger at 100 mtorr than at 400 mtorr ($n_e|_{\rm center}$ at 100 mtorr $= 1.1 \times 10^{15}$ m$^{-3}$ and $n_e|_{\rm center}$ at 400 mtorr $= 3.6 \times 10^{15}$ m$^{-3}$). It should be noted, however, that results from both self-consistent kinetic and fluid simulations of an rf discharge using a benchmark model gas can compare favorably despite differences in the EEDF's [40]. While the reasons for this are not entirely clear, it may be that fluid models, which are conservative equations, when solved self-consistently, tend to redistribute errors in the many approximations and give rise to solutions that are not far from self-consistent kinetic solutions. In Fig. 4

we present the electron heat conduction flux from the simulation $Q_e$, and fluxes assuming Fourier heat conduction $Q_e^{\mathrm{Fo}}$ ($Q_e^{\mathrm{Fo}} = -\kappa_e \partial T_e/\partial x$, $\kappa_e = n_e k^2 T_e/m_e \nu_e$) for the same cases in Fig. 2. The comparison between $Q_e$ and $Q_e^{\mathrm{Fo}}$ is poor at 100 mtorr, whereas there is some qualitative resemblance at 400 mtorr. $Q_e^{\mathrm{Fo}}$ at 100 mtorr changes sign in the central region of the discharge, which corresponds to a minimum in $kT_e$ (Fig. 1), while no such behavior is observed in $Q_e$. From Fig. 3 it is apparent that the portion of the EEDF below $\varepsilon_{\mathrm{ion}}$ for the 100-mtorr case can be represented by a two-temperature Maxwellian. This is a common characteristic of EEDF's in rf discharges at low pressures [28,29,38,39,41,42]. The "fast" or "tail" electron temperature ($\sim$3.5 eV in this case) is characteristic of $kT_e$ in the sheath regions, which is consistent with the observation that it is the fast electrons that interact with the moving electron sheath fronts [39,41,42]. This suggests that the "fast" or "tail" electrons may have a significant effect on $Q_e$ that is not reflected in the gradient of $T_e$. The two-temperature Maxwellian is not prevalent at higher pressures, which is perhaps why there are qualitative similarities between the behavior of $Q_e$ and $Q_e^{\mathrm{Fo}}$ in the 400-mtorr case.

The electron-energy balance [Eq. (4)] for the 12-MHz, 400-mtorr case is shown in Fig. 5 (note that the term corresponding to energy loss due to elastic scattering has been neglected since it is very small). The first inference that we can draw from this figure is that heat conduction [Fig. 5(d)] is an important component of the energy conservation equation. This is true for all the cases considered here. Thus, $\partial Q_e/\partial x$ should not be dropped from

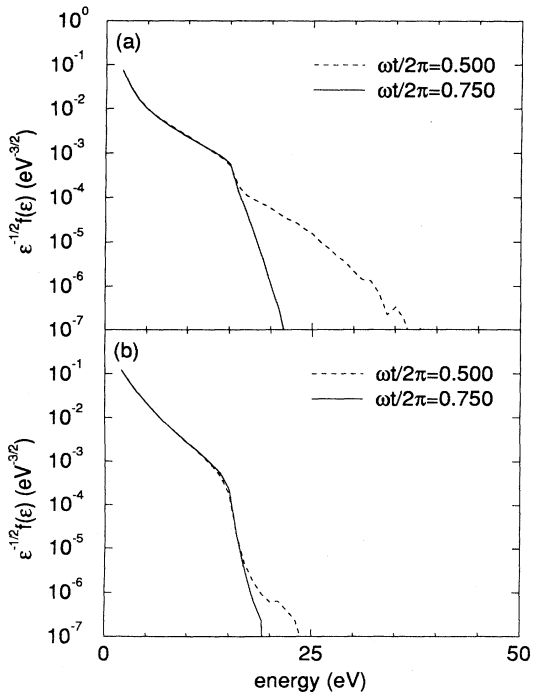


FIG. 3. Electron-energy distribution functions at two times in the rf cycle: (a) 12 MHz, 100 mtorr; and (b) 12 MHz, 400 mtorr.

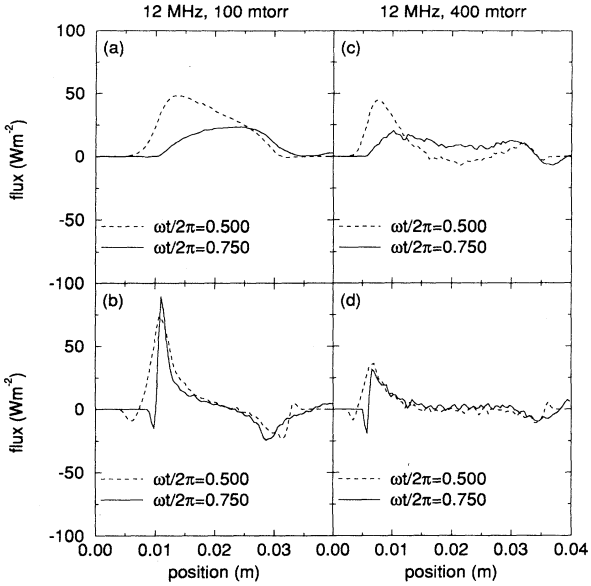


FIG. 4. Heat conduction flux from simulation or calculated assuming Fourier heat conduction: (a) $Q_e$ from simulation (12 MHz, 100 mtorr); (b) $Q_e^{\mathrm{Fo}}$ assuming Fourier heat conduction (12 MHz, 100 mtorr); (c) $Q_e$ from simulation (12 MHz, 400 mtorr); and (d) $Q_e^{\mathrm{Fo}}$ assuming Fourier heat conduction (12 MHz, 400 mtorr). The data are shown at two times in the rf cycle.

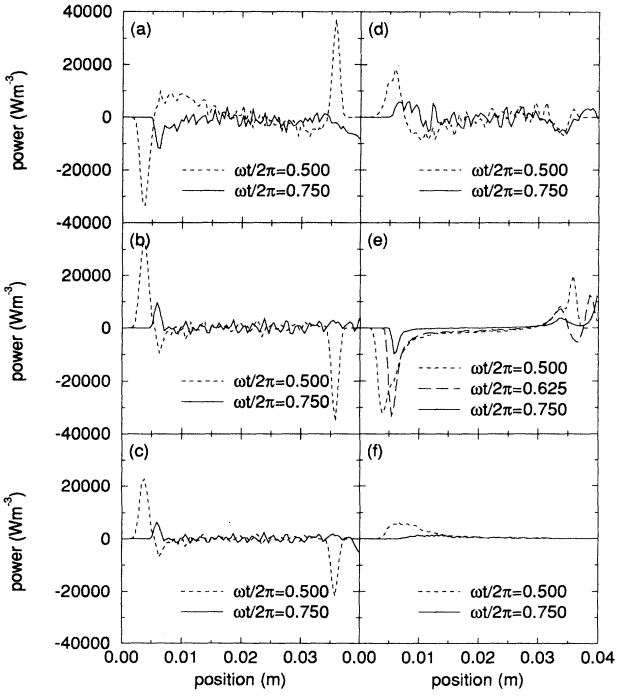


FIG. 5. Terms in the electron-energy balance [Eq. (4)] for the 12-MHz, 400-mtorr case: (a) $\partial(\frac{1}{2} n_e m_e u_e^2 + \frac{3}{2} n_e k T_e)/\partial t$, time derivative; (b) $\partial(\frac{1}{2} n_e m_e u_e^3 + \frac{3}{2} n_e k T_e u_e)/\partial x$, convection; (c) $\partial(n_e k T_{ex} u_e)/\partial x$, pressure work; (d) $\partial Q_e/\partial x$, heat conduction; (e) $e n_e u_e E$, negative of electron heating, i.e., $-j_e E$; and (f) $\varepsilon_{\mathrm{ion}} S_{\mathrm{ion}}$. The data are shown at two times in the rf cycle, except in (e) where an additional curve is shown to indicate electron heating in the anodic phase at the right electrode.

Eq. (4). However, as discussed in the previous paragraph, a good description of $Q_e$ for rf discharges is not known. We also note that some amount of electron heating $j_e E$ [$j_e E = -en_e u_e E$, which is the negative of the quantity that is plotted in Fig. 5(e)] occurs during the retreating phase of the sheath ($\omega_{rf} t/2\pi = 0.625$ at the left electrode). The relative magnitude of this peak (with respect to the heating peak during the sheath expansion) is not as large as that reported by Turner and Hopkins [29]. The maximum field reversal (see $|E_{rev}|$, simulation, in Table I) associated with this peak is also smaller than the results of Turner and Hopkins [29] but is much larger than the field reversal reported by Sommerer *et al.* [22]. Furthermore, this peak is not observed in the cases below 100 mtorr and in simulation results reported for different model gases [25,40]. In the Appendix we present an analysis based on Lieberman's [4] analytic model of a collisional rf sheath and collisional electron transport [c.f. Eq. (13)] which provides a criterion for field reversals and also an estimate of the magnitude of the field.

Results from two cases, 12 MHz, 400 mtorr (Fig. 6) and 30 MHz, 25 mtorr (Fig. 7), are used to demonstrate the effect of pressure and frequency on terms in the electron momentum balance [Eq. (3)]. From Fig. 6 it is apparent that Eq. (12) is quite adequate to describe electron momentum conservation at high pressure. Notice that friction $[n_e m_e \nu_e u_e]$ balances the force term $[en_e E]$ in the central region of the discharge while the pressure gradient $[\partial(n_e kT_e)/\partial x]$ balances the force term in the sheath region. As the pressure is lowered, or conversely as the frequency is increased (Fig. 7), the acceleration term $[\partial(n_e m_e u_e)/\partial t]$ can become significantly larger than the friction term. A simple scaling suggests that Eq. (12) is a reasonable description of electron momentum if $\nu_e \geq \omega_{rf}$ [$\partial(n_e u_e)/\partial t \sim \omega_{rf} n_e u_e$]. We note that the convection term $[\partial(n_e m_e u_e^2)/\partial x]$ is important when there is substantial secondary-electron emission from the electrodes [31].

The plots in Fig. 7 indicate that there are significant oscillations in the bulk of the discharge, especially near the plasma sheath boundary. These oscillations are also present in the 30-MHz, 50-mtorr and 30-MHz, 100-mtorr cases, but decrease with increasing pressure. The presence of these oscillations is reflected in the rf current, which contains high-frequency harmonics. Similar observations have been reported previously [43], and are consistent with results from simulations (almost collisionless) by Vender and Boswell [23,41].

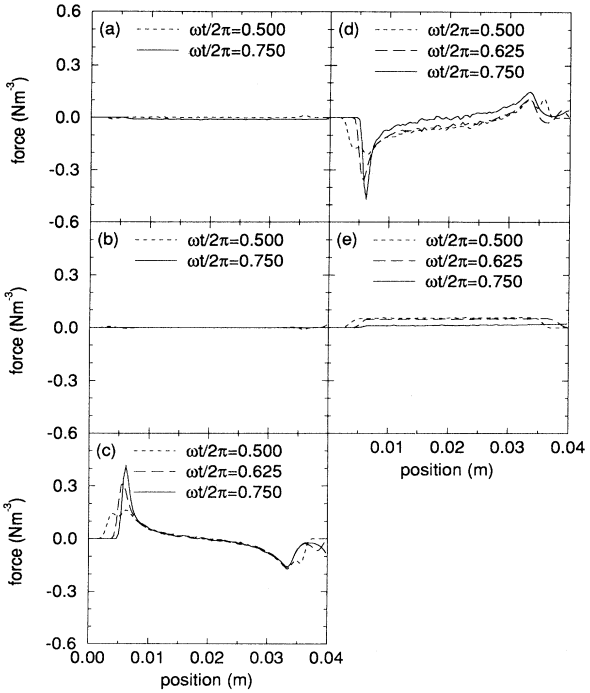


FIG. 6. Terms in the electron momentum balance [Eq. (3)] for the 12-MHz, 400-mtorr case: (a) $\partial(n_e m_e u_e)/\partial t$, acceleration; (b) $\partial(n_e m_e u_e^2)/\partial x$, convection; (c) $\partial(n_e kT_{ex})/\partial x$, pressure; (d) $en_e E$, field force; and (e) $n_e m_e \nu_e u_e$, friction. The data are shown at two times in the rf cycle for (a) and (b); and at three times in the rf cycle for (c), (d), and (e).

TABLE I. Analysis of field reversals for the 12-MHz cases. Note that $\zeta = 0.35$ and $\omega_{rf} = 2\pi \times 12 \times 10^6\ s^{-1}$ have been assumed in these calculations. The pressure is given in units of mtorr.

| Quantity \ Pressure | 100 | 200 | 400 |
|---|---|---|---|
| $j_{rf}$ (A m$^{-2}$) | 9 | 12 | 16 |
| $n_0$ ($10^{15}$ m$^{-3}$) | 0.6 | 1 | 1.5 |
| $kT_{e,avg}$ (eV) | 3 | 3 | 2.5 |
| $\tilde{s}_{e0}$ (mm) | 1.25 | 1 | 0.9 |
| $\lambda_{De0}$ (mm) | 0.5 | 0.4 | 0.3 |
| $\lambda_+$ (mm) | 3.1 | 1.6 | 0.8 |
| $s_m$ (mm) | 12 | 9 | 7 |
| $\omega_{pe0}$ ($10^9$ s$^{-1}$) | 1.4 | 1.8 | 2.2 |
| $\nu_e$ ($10^9$ s$^{-1}$) | 0.16 | 0.32 | 0.64 |
| $H_a$ | 2 | 2 | 2.9 |
| $H_b$ | 1.8 | 1.4 | 1.3 |
| $(\zeta^2/10H_aH_b^2)(\omega_{pe0}^2/\omega_{rf}\nu_e)$ | 0.3 | 0.4 | 0.25 |
| $\|E_{rev}\|$, predicted (V m$^{-1}$) | 280 | 360 | 710 |
| $\|E_{rev}\|$, simulation (V m$^{-1}$) | 160 | 260 | 380 |

### B. Electron power deposition

Electron heating or power deposition in rf discharges has been the subject of considerable interest in recent years [1,3,8,22,29,38,39,41,42,44–47]. Electron heating in rf discharges without any secondary-electron emission is commonly attributed to two mechanisms: (i) bulk heating and (ii) sheath oscillation heating. The former mechanism is attributed to the collisional (or Ohmic) heating of electrons by small electric fields which drive the rf current in the body of the plasma. The latter mechanism is associated with power deposition into electrons by oscillating sheath electric fields [25]. Sheath oscillation heating is generally taken to consist of collisional sheath heating which is essentially no different from collisional bulk heating, and collisionless (non-Ohmic) heating. The collisionless mechanism is often attributed to stochastic heating [5]. Analyses of stochastic heating in the literature typically model the process as electrons reflecting off a moving wall [1,3,44,45]. We note that analytic expressions derived to represent stochastic heating are very sensitive to assumptions that are made about the form of the electron velocity distribution at the moving sheath front. Lieberman [3] assumes that $f(v_{ex},t)=n_{\rm sh}g(v_{ex}-v_{e0})/n_0$, where $g(v_x')$ is a Maxwellian distribution normalized to $n_0$ and $u_{e0}$ is the average electron velocity at the ion sheath edge. $n_0$ is the density at the ion sheath edge and $n_{\rm sh}$ is the density at the moving electron sheath front. $u_{e0}$ is not equal to the velocity of the moving sheath front

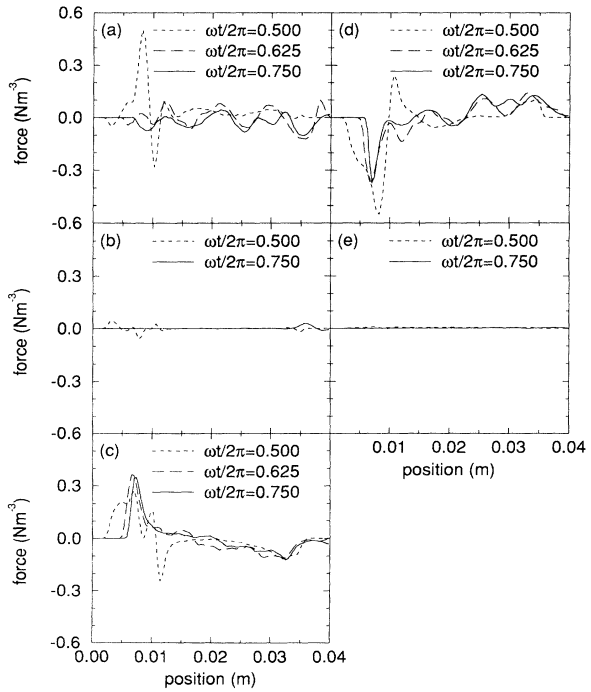


FIG. 7. Terms in the electron momentum balance [Eq. (3)] for the 30-MHz, 25-mtorr case: (a) $\partial(n_em_eu_e)/\partial t$, acceleration; (b) $\partial(n_em_eu_e^2)/\partial x$, convection; (c) $\partial(n_ekT_{ex})/\partial x$, pressure; (d) $en_eE$, field force; and (e) $n_em_e\nu_eu_e$, friction. The data are shown at two times in the rf cycle for (b) and (e); and at three times in the rf cycle for (a), (c), and (d).

$u_{e,\rm sh}$, when the ion density in the sheath region is nonuniform or nonhomogeneous ($n_{\rm sh}\neq n_0$). Using this distribution, an expression for power deposition is derived. This expression vanishes for the case where ion density in the sheath is uniform, suggesting that there is no stochastic heating in the homogeneous ion sheath model [3,45]. However, if $f(v_{ex},t)$ is assumed to be equal to $n_{\rm sh}g(v_{ex}-u_{e,\rm sh})/n_0$, which is consistent with electron current continuity behind the moving sheath front [$n_0u_{e0}=n_{\rm sh}u_{e,\rm sh}$, which comes from Eq. (2) with $\partial n_e/\partial t$ and $S_{\rm ion}$ set to zero], then the expression for power transfer vanishes even with a nonuniform ion density in the sheath. If, on the other hand, $f(v_{ex},t)=n_{\rm sh}g(v_{ex})/n_0$ is assumed [1], then the expression predicts that there is power transfer with both homogeneous and nonhomogeneous sheaths. Nonetheless, simulations that do not include scattering collisions suggest that collisionless heating is present in rf discharges [23]. Vender and Boswell [41] suggest that beam plasma instabilities may play an important role in sheath power transfer.

In this section we attempt to examine the importance of collisional and collisionless heating in rf discharges. A time-averaged electron mechanical energy balance can be obtained by multiplying the electron momentum balance [Eq. (3), using Eq. (8)] with $u_e$ and averaging over time,

$$\overline{u_e\frac{\partial(n_em_eu_e)}{\partial t}}+\overline{u_e\frac{\partial(n_em_eu_e^2)}{\partial x}}+\overline{u_e\frac{\partial(n_ekT_{ex})}{\partial x}}+\overline{n_em_e\nu_eu_e^2}+\overline{en_eu_eE}=0\ . \quad (17)$$

The time-averaged electron heating $\overline{j_eE}$ is given by $-\overline{en_eu_eE}$. The collisional or Ohmic heating term $\overline{n_em_e\nu_eu_e^2}$ can be written as $\overline{j_e^2R_{\rm Ohm}}$, where $R_{\rm Ohm}=m_e\nu_e/e^2n_e$. The first three terms on the left-hand side of Eq. (17) can be identified with the collisionless (or non-Ohmic) contributions to $\overline{j_eE}$. In Fig. 8 we show the five components of the time-averaged electron mechanical energy balance [Eq. (17)]. Note that electron heating ($\overline{j_eE}$) is denoted by negative values of the field term in Fig. 8. The first observation that can be made is that electron heating can be approximately expressed as the sum of a pressure contribution and a collisional contribution,

$$\overline{j_eE}=\overline{u_e\frac{\partial(n_ekT_{ex})}{\partial x}}+\overline{j_e^2R_{\rm Ohm}} \quad (18)$$

which is consistent with Eq. (12). For the cases considered here, the pressure contribution is important at lower gas pressure ($\leq 100$ mtorr), while collisional heating is dominant at higher gas pressure. The collisionless component of $j_eE$ can, at least from a fluid standpoint be associated with work done in compression (sheath expansion) and rarefaction (sheath collapse) of the electron gas. We note that if the compression and rarefaction of the electron gas is done reversibly, then $u_e\partial(n_ekT_{ex})/\partial x$ would time average to zero. However, the process is not reversible since there are other loss mechanisms for electron energy density, such as ionization and electron loss to electrodes. The plots in Fig. 8 show that the pressure contribution to $j_eE$ is positive through most of the sheath

while it is negative in the quasineutral part of the discharge. It is also negative in the region immediately adjacent to the electrodes, which is related to diffusion cooling as electrons are lost to the surface. The importance of electron pressure effects in reducing $(j_e E)$ in the central region of the discharge has been discussed in a previous work [39]. The model presented by Surendra and Graves [39] is not used to analyze the results presented here since the model is designed primarily for cases with two-temperature EEDF's where the fast electron temperature is much larger than the slow electron temperature [48]. The collisional component of $j_e E$ also peaks in the sheath (Fig. 8). This is because the lower density in the sheath leads to a larger $R_{\mathrm{Ohm}}$ which more than offsets the effect of spatially and temporally varying $j_e$. The behavior of the pressure contribution is less easy to understand. Analytic models of the rf sheath [3] indicate that $u_e \partial(n_e k T_{ex})/\partial x$ is zero, since in these models sheath expansion is symmetric with sheath collapse and $kT_{ex}$ is constant (i.e., reversible). Note that the acceleration and convection terms similarly average to zero. To illustrate the crucial role of the time and space variation of $kT_{ex}$ we show in Fig. 9 $u_e \partial(n_e k T_{ex})/\partial x$ and $kT_{e,\mathrm{avg}} u_e \partial n_e/\partial x$ where $kT_{e,\mathrm{avg}}$ is set at 2 eV [c.f. Eq. (13)]. The latter expression is negative throughout the entire region of the discharge. This indicates that the collisionless component of $j_e E$ cannot be captured by using the simple drift-diffusion approximation for $j_e$ [Eq. (13)].

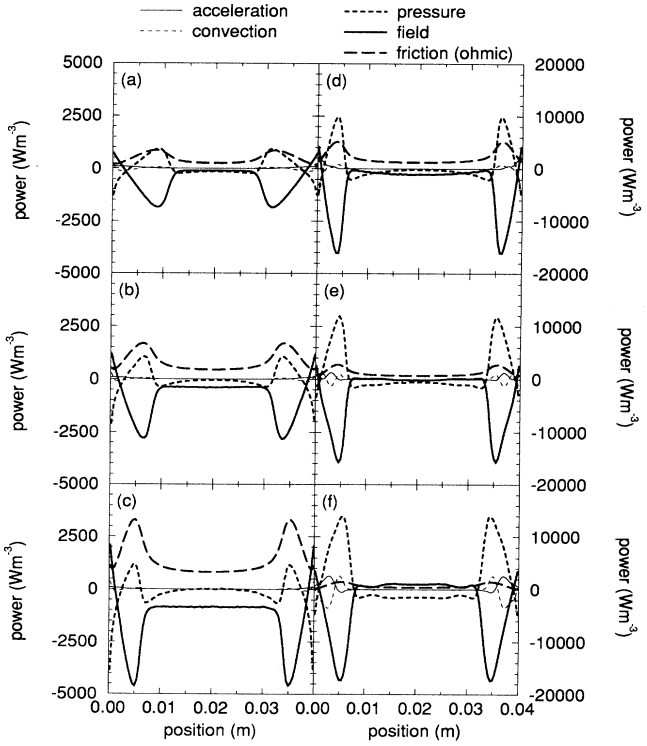


FIG. 8. Terms in the time-averaged electron mechanical energy balance [Eq. (17)]: (a) 12 MHz, 100 mtorr; (b) 12 MHz, 200 mtorr; (c) 12 MHz, 400 mtorr; (d) 30 MHz, 100 mtorr; (e) 30 MHz, 50 mtorr; and (f) 30 MHz, 25 mtorr. Acceleration term (thin solid line); convection term (thin short-dashed line); pressure term (thick short-dashed line); field term or negative of electron heating, $-j_e E$ (thick solid line); and friction or collisional term (thick long-dashed line).

### C. Ion moments

We now consider the ion moments of interest to fluid simulations. Ion "$x$ temperature" $kT_{+x}$, and drift energy $\frac{1}{2} m_+ u_+^2$, for the 12-Mhz, 100-mtorr, and 12-MHz, 400-mtorr cases are shown in Fig. 10. In the central region of the discharge $\frac{1}{2} m_+ u_+^2 \ll kT_{+x} \approx kT_n$. Equation (14), which suggests $\frac{1}{2} m_+ u_+^2 \approx kT_{+x}$, does not fit the simulation results particularly well since Eq. (14) is valid for situations where $kT_n = 0$, whereas $kT_n = 0.026$ eV in the PIC-MCC simulation. Furthermore, it does not apply in the sheath regions where $\frac{1}{2} m_+ u_+^2$, $kT_{+x} \gg kT_n$ since the acceleration $[\partial(n_+ m_{e+} u_+)/\partial t]$ term in the ion momentum balance [Eq. (7)] is not small here. We also note that the ion drift velocity at the sheath edge in these simulations is about a factor of 3 smaller than the modified ion sound speed suggested by Godyak and Sternberg [2]. These observations are consistent with results reported by Sommerer *et al.* [22]. The modified sound speed which is derived for a collisional dc sheath may have limited applicability for rf sheaths with significant temporal modulation of ion velocity (this is

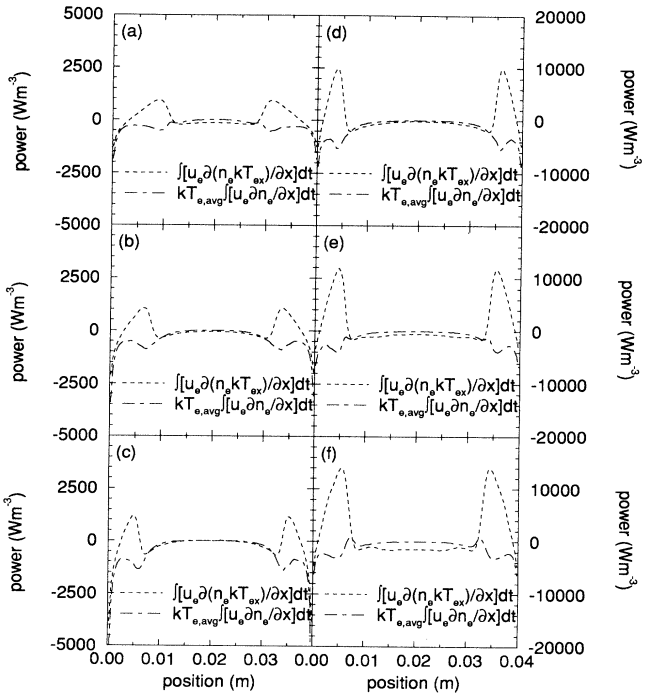


FIG. 9. Comparison of pressure terms in the time-averaged electron mechanical energy balance: (a) 12 MHz, 100 mtorr; (b) 12 MHz, 200 mtorr; (c) 12 MHz, 400 mtorr; (d) 30 MHz, 100 mtorr; (e) 30 MHz, 50 mtorr; and (f) 30 MHz, 25 mtorr. Pressure term from simulation, $u_e \partial(n_e k T_{ex})/\partial x$ (short-dashed line); and pressure term assuming a time- and space-invariant electron temperature, $kT_{e,\mathrm{avg}} u_e \partial n_e/\partial x$ short-dashed long-dashed line).

typically seen with light ions or thin sheaths).

In Figs. 11 and 12 we show the various components in the ion momentum balance [Eq. (7)] for the 12-MHz, 400-mtorr and 30-MHz, 25-mtorr cases, respectively. At higher pressures the field force term is balanced by the acceleration and friction terms, whereas at lower pressures the convection becomes important. A simple scaling analysis of the friction $[n_+ m_+ n_n \sigma_{\rm chx} \langle v_{+x} | v_{+x} | \rangle \sim n_+ m_+ n_n \sigma_{\rm chx} u_+^2]$ and convection $[\partial(n_+ m_+ u_+^2)/\partial x \sim n_+ m_+ u_+^2 / s_m]$ terms in the sheath region suggests that the convection term should be retained in the momentum balance when the sheath thickness $s_m$ is such that $s_m \leq \lambda_+$, the ion mean path $(1/n_n \sigma_{\rm chx})$. The results also suggest that the pressure term can be safely ignored in the ion momentum balance. Note, however, that the drift-diffusion approximation for ions [Eq. (15)] is not particularly accurate since the acceleration term is not small in comparison to the friction term $(\omega_{\rm rf} > u_+ / \lambda_+)$.

### D. Summary and conclusions

Moments of the Boltzmann equation have been calculated for electron and ion transport using a PIC-MCC simulation. The results indicate simple models for the higher moments such as heat conduction and ionization rate can contain significant errors since the behavior of the EEDF is complicated. Nonetheless heat conduction is an important component of the electron-energy balance. The assumption that for electrons, $kT_{\rm ex} \approx kT_e \gg \frac{1}{2} m_e u_e^2$ is generally quite good. While the assumption that $kT_{+x} \approx kT_n$ is not valid for ions in the sheath, this approximation does not have any significant impact since the pressure term in the ion momentum balance is generally unimportant.

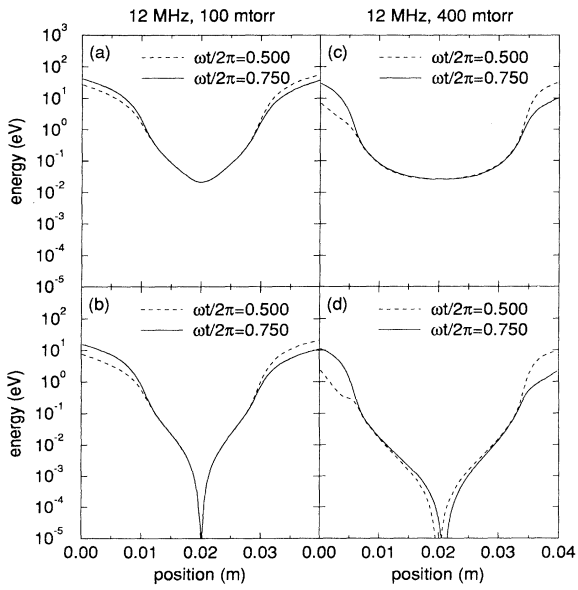


FIG. 10. Ion "$x$ temperature" and drift energy: (a) $kT_{+x}$ (12 MHz, 100 mtorr); (b) $\frac{1}{2} m_+ u_+^2$ (12 MHz, 100 mtorr); (c) $kT_{+x}$ (12 MHz, 400 mtorr); and (d) $\frac{1}{2} m_+ u_+^2$ (12 MHz, 400 mtorr). The data are shown at two times in the rf cycle.

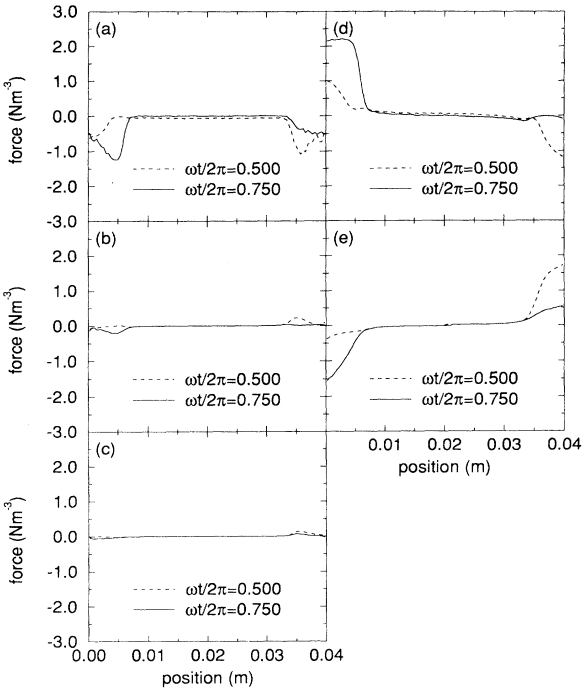


FIG. 11. Terms in the ion momentum balance [Eq. (7)] for the 12-MHz, 400-mtorr case: (a) $\partial(n_+ m_+ u_+)/\partial t$, acceleration; (b) $\partial(n_+ m_+ u_+^2)/\partial x$, convection; (c) $\partial(n_+ kT_{+x})/\partial x$, pressure; (d) $-en_+ E$, field force; and (e) $n_+ m_+ n_n \sigma_{\rm chx} \langle v_{+x} | v_{+x} | \rangle$, friction. The data are shown at two times in the rf cycle.

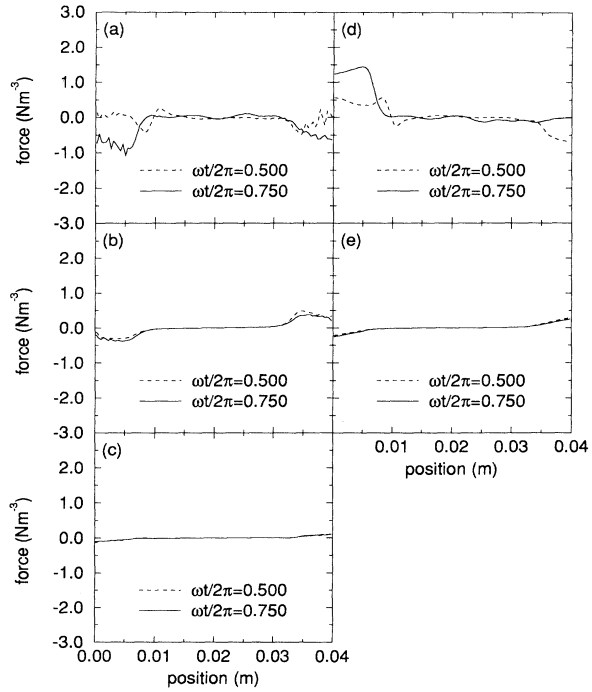


FIG. 12. Terms in the ion momentum balance [Eq. (7)] for the 30-MHz, 25-mtorr case: (a) $\partial(n_+ m_+ u_+)/\partial t$, acceleration; (b) $\partial(n_+ m_+ u_+^2)/\partial x$, convection; (c) $\partial(n_+ kT_{+x})/\partial x$, pressure; (d) $-en_+ E$, field force; and (e) $n_+ m_+ n_n \sigma_{\rm chx} \langle v_{+x} | v_{+x} | \rangle$, friction. The data are shown at two times in the rf cycle.

The convection term in the electron momentum balance can be neglected for systems where secondary-electron emission is not significant. This term is important in the ion momentum balance if the collisionality of the sheaths is low. The acceleration term in both balances is important when the collision frequency is on the order of the rf frequency.

Examination of the time-averaged electron mechanical energy balance (product of $u_e$ with the electron momentum balance) indicates that the major component of collisionless (or non-Ohmic) heating in $j_e E$ is associated with the pressure term. The spatial and temporal variation of the electron temperature in the pressure term ($n_e k T_{ex}$) is an integral component of this collisionless heating and should be retained.

The results presented here suggest that calculating moments of various quantities in a kinetic simulation can not only provide information that is valuable to fluid approaches but also useful insight into discharge characteristics.

## ACKNOWLEDGMENTS

The authors are very grateful to B. M. Penetrante for calculating swarm parameters using the model-gas cross sections. The authors also acknowledge useful discussions with D. Vender, R. T. Farouki, and S. Hamaguchi. Computations were done on IBM RISC System/6000 computer workstations supported by the High Performance Computing Group at IBM T. J. Watson Research Center.

## APPENDIX: FIELD REVERSALS IN THE SHEATH

Following Lieberman [4] we assume that the moving electron sheath front oscillates between the ion sheath edge and the electrode wall (Fig. 1 in Ref. [4]). All the rf current $j_{rf}$ on the plasma side of the moving electron sheath front is carried by the electrons. At high pressures the drift-diffusion approximation for electrons is appropriate, hence we can write the electron current as [Eq. (13)]

$$j_e = e\mu_e n_e E + eD_e \frac{\partial n_e}{\partial x} . \tag{A1}$$

During the retreating phase of the sheath, a field reversal which pushes electrons towards the electrode will occur if the diffusive current anywhere in the region between the ion sheath edge and the moving electron sheath front is insufficient to provide the total rf current, i.e.,

$$R = \left| eD_e \left[ \frac{\partial n_e}{\partial x} \right] \Big/ j_{rf} \right| < 1 . \tag{A2}$$

This ratio $R$ is smallest at the moving electron sheath front. On the plasma side of the moving electron sheath front $n_e = n_+$. Thus, by using the expressions for $n_+$ and other relevant quantities in Ref. [4], $R$ can be obtained. For the purposes of the calculations here, the ions are assumed to enter the sheath with a velocity of $\zeta u_B$, where $u_B$ is the Bohm velocity $(kT_{e,\text{avg}}/m_+)^{1/2}$ and $\zeta$ is a correction factor. For example, if Godyak and Sternberg's [2] modified ion sound speed for collisional sheaths is used, then $\zeta = (1+\pi\lambda_{De0}/2\lambda_+)^{-1/2}$, where the electron Debye length is given by $\lambda_{De0} = (\varepsilon_0 kT_{e,\text{avg}}/e^2 n_0)^{1/2}$ and $n_0$ is the density at the ion sheath edge, while $\lambda_+$ is ion mean free path $(1/n_n \sigma_{\text{chx}})$. Results presented here (see Sec. V C) and elsewhere [22] indicate that $\zeta$ can be significantly less than 1 ($\zeta \sim 0.35$),

$$R = \zeta^2 \frac{\omega_{pe0}^2}{\omega_{rf}\nu_e} \frac{\pi^2 \lambda_{De0}^4}{4\tilde{s}_{e0}^3 \lambda_+} \frac{\phi}{\sin(\phi)(\sin\phi - \phi\cos\phi)^2} . \tag{A3}$$

In the above equation the electron plasma frequency is given by $\omega_{pe0} = (e^2 n_0/\varepsilon_0 m_e)^{1/2}$, and the electron oscillation amplitude at the ion sheath edge is given by $\tilde{s}_{e0} = \tilde{J}_{rf}/e\omega_{rf} n_0$, where $\tilde{J}_{rf}$ is the rf current amplitude. $\phi$ $(0 \le \phi \le \pi)$ is defined as the phase at which the moving electron sheath front is at position $x$ (see Fig. 2 in Ref. [4]). The smallest value of the ratio in Eq. (A3) ($R_{\min}$) occurs when $\phi = 2.35$ rad $\approx 3\pi/4$ [which corresponds to $\omega_{rf} t/2\pi = 0.625$ in Fig. 5(e)]and is approximately given by

$$R_{\min} \approx \frac{\zeta}{10 H_a H_b^2} \frac{\omega_{pe0}^2}{\omega_{rf}\nu_e} , \tag{A4}$$

where we have used dimensionless quantities $H_a = \tilde{s}_{e0}^2/\pi\lambda_{De0}^2$, $H_b = (2\lambda_+ \tilde{s}_{e0}/\pi^2 \lambda_{De0}^2)^{1/2}$ as defined by Lieberman [3,4]. Thus, if $R_{\min}$ is less than 1, then a field reversal is expected. The magnitude of the field can be obtained with Eq. (A1),

$$|E_{\text{rev}}| \approx \frac{j_{rf}}{e\mu_e n_{\text{sh}}} \left[ 1 - \frac{\zeta^2}{10 H_a H_b^2} \frac{\omega_{pe0}^2}{\omega_{rf}\nu_e} \right] , \tag{A5}$$

where $n_{\text{sh}}$ is the density at the moving electron sheath front. Using $s_m \approx 1.95 H_b s_{e0}/\zeta$, where $s_m$ is the ion sheath thickness [4] and $\phi = 2.35$ rad, we obtain

$$|E_{\text{rev}}| \approx \frac{m_e s_m \omega_{rf}\nu_e}{2e} \left[ 1 - \frac{\zeta^2}{10 H_a H_b^2} \frac{\omega_{pe0}^2}{\omega_{rf}\nu_e} \right] . \tag{A6}$$

If $(\zeta^2/10 H_a H_b^2)(\omega_{pe0}^2/\omega_{rf}\nu_e) \ll 1$, then this result is the same as the expression presented by Turner and Hopkins [29]. Results of the above analysis for the 12-MHz cases are shown in Table I. The predicted values of $|E_{\text{rev}}|$ are within a factor of 2 of the values in the simulation. This is reasonably good agreement considering the number of assumptions that are built into the analysis.

A similar analysis can be done for a collisionless rf sheath [3], however, Eq. (A1) is not accurate in the collisionless regime. The analysis presented by Vender and Boswell [41] is more appropriate in the collisionless regime.

[1] V. A. Godyak, *Soviet Radiofrequency Research* (Delphic, Falls Church, VA, 1986); V. A. Godyak, Fiz. Plazmy **2**, 141 (1976) [Sov. J. Plasma Phys. **2**, 78 (1976)]; Zh. Tekh. Fiz. **41**, 849 (1971) [Sov. Phys. Tech. Phys. **16**, 1073 (1972)].
[2] V. A. Godyak and N. Sternberg, Phys. Rev. A **42**, 2229 (1990); IEEE Trans. Plasma Sci. **18**, 159 (1990).
[3] M. A. Lieberman, IEEE Trans. Plasma Sci. **16**, 638 (1988).
[4] M. A. Lieberman, IEEE Trans. Plasma Sci. **17**, 338 (1989).
[5] G. R. Misium, A. J. Lichtenberg, and M. A. Lieberman, J. Vac. Technol. Sci. A **7**, 1007 (1989).
[6] D. B. Graves and K. F. Jensen, IEEE Trans. Plasma Sci. **PS-14**, 78 (1986).
[7] J. P. Boeuf, Phys. Rev. A **36**, 2782 (1987).
[8] Ph. Belenguer and J. P. Boeuf, Phys. Rev. A **41**, 4447 (1990).
[9] M. S. Barnes, T. J. Cotler, and M. E. Elta, J. Comput. Phys. **77**, 53 (1988).
[10] V. V. Boiko, Yu. A. Mankelvich, A. T. Rakhimov, N. T. Suetin, V. A. Feoktistov, and S. S. Filipov, Fiz. Plazmy **15**, 867 (1989) [Sov. J. Plasma Phys. **15**, 504 (1989)].
[11] J. H. Tsai and C. Wu, Phys. Rev. A **41**, 5626 (1990).
[12] S. K. Park and D. J. Economou, J. Appl. Phys. **68**, 3094 (1990).
[13] Y. H. Oh, N. H. Choi, and D. I. Choi, J. Appl. Phys. **67**, 3264 (1990).
[14] A. P. Paranjpe, J. P. McVittie, and S. A. Self, Phys. Rev. A **41**, 6949 (1990).
[15] M. Meyyappan, J. Appl. Phys. **69**, 8047 (1991).
[16] E. Gogolides, H. H. Sawin, and R. A. Brown, Chem. Eng. Sci. **47**, 3839 (1992).
[17] T. Makabe, N. Nakano, and Y. Yamaguchi, Phys. Rev. A **45**, 2520 (1992).
[18] N. Sato and H. Tagashira, IEEE Trans. Plasma Sci. **19**, 102 (1991).
[19] T. J. Sommerer and M. J. Kushner, J. Appl. Phys. **71**, 1564 (1992).
[20] J. P. Boeuf and Ph. Belenguer, J. Appl. Phys. **71**, 4751 (1992).
[21] M. E. Riley, P. Drallos, and R. McGrath, Bull. Am. Phys. Soc. **37**, 1922 (1992).
[22] T. J. Sommerer, W. N. G. Hitchon, R. E. P. Harvey, and J. E. Lawler, Phys. Rev. A **43**, 4452 (1991).
[23] D. Vender and R. W. Boswell, IEEE Trans. Plasma Sci. **18**, 725 (1990).
[24] M. Surendra, D. B. Graves, and I. J. Morey, Appl. Phys. Lett. **56**, 1022 (1990).
[25] M. Surendra and D. B. Graves, IEEE Trans. Plasma Sci. **19**, 144 (1991).
[26] C. K. Birdsall, IEEE Trans. Plasma Sci. **19**, 65 (1991).
[27] H. W. Trombley, F. L. Terry, Jr., and M. E. Elta, IEEE Trans. Plasma Sci. **19**, 158 (1991).
[28] V. Vahedi, C. K. Birdsall, M. A. Lieberman, G. DiPeso, and T. G. Rognlien, Phys. Fluid B **5**, 2719 (1993).
[29] M. M. Turner and M. B. Hopkins, Phys. Rev. Lett. **69**, 3511 (1992).
[30] A. Date, K. Kitamori, Y. Sakai, and H. Tagashira, J. Phys. D **25**, 442 (1992).
[31] M. Dalvie, R. T. Farouki, S. Hamaguchi, and M. Surendra, J. Appl. Phys. **72**, 2620 (1992).
[32] R. T. Farouki, S. Hamaguchi, and M. Dalvie, Phys. Rev. A **44**, 2664 (1991).
[33] M. Hayashi, Institute of Plasma Physics, Nagoya University, Report No. IPPJ-AM-19, 1981 (unpublished).
[34] M. Meyyappan and J. P. Kreskovsky, J. Appl. Phys. **68**, 1342 (1990).
[35] P. Bayle, J. Vacquie, and M. Bayle, Phys. Rev. A **34**, 360 (1986).
[36] J. E. Lawler, Phys. Rev. A **32**, 2977 (1985).
[37] B. M. Penetrante (personal communication). Swarm parameters are obtained with a Boltzmann code described in W. L. Morgan and B. M. Penetrante, Comput. Phys. Commun. **58**, 127 (1990).
[38] V. A. Godyak, R. B. Piejak, and B. M. Alexandrovich, Plasma Sources Sci. Technol. **1**, 36 (1992).
[39] M. Surendra and D. B. Graves, Phys. Rev. Lett. **66**, 1469 (1991).
[40] M. Surendra (unpublished).
[41] D. Vender and R. W. Boswell, J. Vac. Technol. Sci. A **10**, 1331 (1992).
[42] B. P. Wood, M. A. Lieberman, and A. J. Lichtenberg, Bull. Am. Phys. Soc. **37**, 1912 (1992).
[43] D. B. Graves and M. Surendra (unpublished).
[44] C. G. Goedde, A. J. Lichtenberg, and M. A. Lieberman, J. Appl. Phys. **64**, 4375 (1988).
[45] I. G. Kaganovich and L. Tsendin, IEEE Trans. Plasma Sci. **20**, 86 (1992).
[46] A. E. Wendt and W. N. G. Hitchon, J. Appl. Phys. **71**, 4718 (1992).
[47] M. J. Kushner, IEEE Trans. Plasma Sci. **PS-14**, 188 (1986).
[48] M. Surendra, Ph.D. thesis, University of California, Berkeley, CA, 1991 (unpublished).